

# Edge states mechanism for the anomalous quantum Hall effect in diatomic square lattice

B. Ostahie, M. Niță, and A. Aldea

National Institute of Materials Physics, POB MG-7, 77125 Bucharest-Magurele, Romania

(Dated: May 15, 2018)

The understanding of the Chern insulator and anomalous quantum Hall effect (AQHE) in terms of chiral edge states in confined systems is the first aim of the paper. The model we use consists in a diatomic square lattice with hopping to the next-nearest-neighbors and broken time-reversal symmetry, which exhibits edge states in the absence of an external magnetic field. The question of chiral edge states is approached in the ribbon and plaquette geometries with different atomic connectivities at the boundaries. Insulating and semimetallic phases are revealed, the resulting phase diagram being richer than in Haldane's model. The transmission coefficients and the Hall resistance  $R_H$  are calculated for the finite size system in the Landauer-Büttiker formalism. The quantized values  $R_H = \pm h/e^2$ , specific to the Chern insulator, are manifest in the energy range occupied by the chiral edge states, corresponding to the unique gap existing in the energy spectrum. Our second aim is to examine the disorder-induced properties of the model, and, as a novelty, we prove the *disorder-driven* AQHE in the semimetallic phase.

## INTRODUCTION

The paradigm of the anomalous quantum Hall effect was advanced by Haldane for a hexagonal lattice model by imposing two *sine qua non* conditions: i) the hopping process to the next-nearest-neighbors (n.n.n), and ii) the phase attached to this process. The phase is justified in terms of a periodic internal magnetic field, chosen such that the flux through the unit cell vanishes. The phase diagram of the model contains domains with topological properties, where the Chern number is  $\nu = \pm 1$ . Such systems, which may support quantum Hall effect in the absence of an external magnetic field, have been called Chern insulators. The topic has been developed next to account for the robustness of the effect in the presence of disorder [2, 3], and for the interactions in the fractional anomalous quantum Hall effect [4, 5]. The same model has been extended by Kane and Mele by adding the spin-orbit coupling and proving theoretically the quantum spin Hall effect [8]. The case of the edge states in the Haldane's honeycomb model has been invoked in [6, 7].

In principle, by virtue of the bulk-edge correspondence [9], alternatively to the approach based on topological invariants (which assumes Bloch functions and works for *infinite* systems), the topological properties can be addressed in terms of chiral edge states existing in *finite* systems.

This paper aims to detect chiral edge states, assumed to exist at vanishing magnetic flux under specific conditions and to support anomalous quantum Hall effect in Chern insulators. The confirmation of such states provides more physical insight into this effect, and it is by itself an interesting issue that certifies the bulk-edge correspondence also in this case.

Next, the paper observes the presence of a semimetallic phase where edge states are intercalated with bulk states.

By the use of disorder, we localize the bulk and activate the edge states, which prove to be robust and to support quantized transport. This result advances the new conceptual issue of the *disorder-driven* anomalous quantum Hall effect.

The diatomic square lattice with nearest-, and next-nearest-neighbor hopping [10] is a rich model exhibiting different phases: semimetallic (SM), band insulating (BI), and Chern insulating (CI). Recently, this lattice was also considered to advocate the presence of spin-polarized flat bands in topological crystalline insulators [11]. The model consists of two square lattices built of atoms  $A$  or  $B$ , respectively, interconnected by a complex nearest-neighbor hopping term  $t_{AB} = t_1 e^{i\gamma}$ . So far the lattice is bipartite, however the model is completed with the next-nearest-hopping  $t_{AA} = t_{BB} = t_2$  that breaks this property by connecting atoms of the same type.

Being known that the bipartite symmetry of a lattice ensures the electron-hole symmetry of the energy spectrum [12], the present model is an unexpected example that exhibits the spectral symmetry in the absence of the lattice bipartitism (see Eq.(8)).

The breaking of the time-reversal (TR) symmetry, necessary for the appearance of the Hall effect, comes from the phase  $\gamma$  attached to the n.n. hopping parameter  $t_1$ . It turns out, however, that the condition  $\gamma \neq 0$  by itself is not sufficient to get topological states, and the presence of the n.n.n. hopping parameter  $t_2 \neq 0$  is also necessary.

Different phases (SM, BI, CI) can be identified at once from the expression of the energy spectrum Eq.(8), which is obtained easily using the Fourier transform of the Hamiltonian describing the infinite lattice. Beside  $t_1, t_2$  and  $\gamma$ , a fourth parameter proves to be important, namely the energy spacing  $\Delta = (E_a - E_b)/2$  (where  $E_a, E_b$  are the site energies in the Hamiltonian (1)).

The evidence of the edge states is more conveniently studied in the ribbon (strip) geometry, in which case ana-

lytic calculations are also accessible. On the other hand, the study of the transport properties, and, in particular, the calculation of the Hall conductance in the topological phase, requires a plaquette geometry.

The ribbons are tailored by cutting the edges along different directions in the lattice. Since the edges may show different atomic connectivities, the ribbons may also differ in their spectral properties. Edges parallel to A-A and A-B directions in the diatomic lattice (see Fig.1) are considered in Sec.III. The location of the edge states along the ribbon boundaries is attested analytically and numerically.

The ribbon energy spectrum may be gapped, corresponding to conventional (bulk) insulators, if the gap is empty, or to topological insulators, if the gap is filled with edge states. A semimetallic phase containing edge states is also found. In this case, depending on parameters, the edge states are organized as a flat band located in the middle of the spectrum (similar to the zig-zag graphene ribbon), or may be dispersive. The second case is more exotic. The point is that the dispersive edge states are embedded in the continuum of the bulk states, as evident in Fig.5a and Fig.5b. The issue of the disorder-driven topological phase, discussed in Sec.IV, is based on this observation.

The finite plaquette is obtained by imposing vanishing boundary conditions all around the perimeter. The description of the energy spectrum as function of the phase  $\gamma$  is the analogue of the Hofstadter-type spectrum for the confined 2D electron gas, expressed in terms of the external magnetic flux. Although both spectra contains edge states, there are striking differences. The Hofstadter butterfly contains a sequence of bands and gaps originating in the Landau levels. By imposing boundaries, the gaps get filled with edge states, whose chirality is given by the derivative of the eigenenergies with respect to the magnetic flux. In contrast, the energy spectrum of the finite square diatomic lattice contains a single gap, which accommodates edge states and exhibits a 'binocular' aspect (see Fig.9b). The proof of chirality should be addressed however differently [13], and it can be done either by calculating the diamagnetic moments associated to the edge states or showing the asymmetric behavior of the transmission coefficients in the Landauer-Büttiker approach [14]. The second route will be followed in Sec.IV of the paper.

The edge states embedded in the multitude of bulk states, discovered first for the ribbon geometry, deserves special attention in the case of plaquettes. Being masked by the bulk states, they cannot be observed in the transport, and, in order to evidenciate their contribution, one has to find the proper tool to obstruct the states in the bulk. The question is addressed in Sec.IV. in the frame of disorder induced localization.

The surprising result is that, by increasing gradually the disorder, the quantized Hall resistance  $R_H = \pm h/e^2$

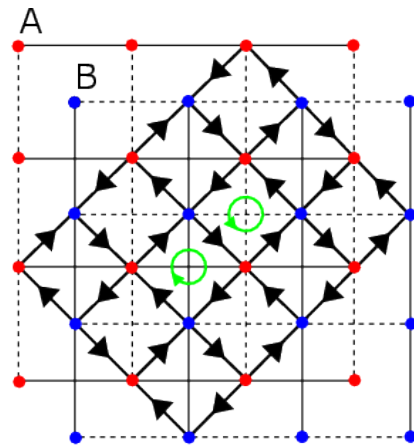


FIG. 1: (Color online) Diatomic square lattice structure: A and B atoms are interconnected by the hopping  $t_1$  carrying the phase  $\gamma$  (represented by black arrows). The green arrows indicate the phase loops in the lattice. The A-A and B-B hopping parameter  $t_2$  is real, but taken with positive/negative sign along the solid/dashed lines.

becomes manifest, as shown in Fig.12. This outcome demonstrates that the edge states survive to disorder, while the states in the bulk get localized, being unable to participate in the transport. This proves that the novel edge states, identified in the semimetallic phase, are chiral topological states, able to support the anomalous quantum Hall effect.

The transport calculations are performed numerically in the Landauer-Büttiker approach [14], which pretends the knowledge of the Green function corresponding to the full Hamiltonian describing the sample, the leads and the coupling between them.

The model Hamiltonian, its symmetries, and possible phases are detailed in Sec.II. Section III is devoted to spectral properties in the ribbon geometry, with focus on the edge states. The spectral and transport properties of the clean and disordered plaquettes, with focus on the Hall resistance quantization in the Chern insulating phase are discussed in Sec.IV. The conclusions are summarized in the last section.

## THE HAMILTONIAN, SYMMETRIES AND SPECTRAL PROPERTIES

We consider the square lattice with two atoms A and B per the unit cell defined by the primitive vectors  $\vec{a}_1, \vec{a}_2$ . Let us introduce the creation (annihilation) operators  $a_{nm}^\dagger, b_{nm}^\dagger (a_{nm}, b_{nm})$ , corresponding to the atoms in the unit cell specified by the lattice vector  $\vec{R}_{nm} = n\vec{a}_1 + m\vec{a}_2$ .

We shall analyze the spectral and topological transport properties of systems described by the following tight-

binding model Hamiltonian [10]:

$$\begin{aligned}
H = & \sum_{n,m} [E_a a_{nm}^\dagger a_{nm} + E_b b_{nm}^\dagger b_{nm}] \\
& - t_1 \sum_{n,m} [e^{-i\gamma} a_{nm}^\dagger (b_{nm} + b_{n-1,m-1}) \\
& + e^{i\gamma} a_{nm}^\dagger (b_{n,m-1} + b_{n-1,m}) + H.c.] \\
& - t_2 \sum_{n,m} [a_{nm}^\dagger (a_{nm+1} - a_{n+1,m}) \\
& - b_{nm}^\dagger (b_{nm+1} - b_{n+1,m}) + H.c.] , \quad (1)
\end{aligned}$$

where  $E_a, E_b$  are site energies, and  $t_1, t_2$  are the nearest-neighbor and next-nearest-neighbor hopping parameters. Associated to  $t_1$ , the phase  $\gamma$  can be considered as resulting from a periodic magnetic field (as in Haldane's picture [1]), which does not generate any flux through the unit cell.

As usual, the Fourier transform  $a_{nm} = \sum_{\vec{k}} a_{\vec{k}} e^{i\vec{k}\vec{R}_{nm}}$  (and similarly for  $b_{nm}$ ) helps in the Hamiltonian diagonalization. With the choice of  $\vec{a}_1$  and  $\vec{a}_2$  as in Fig.3a, the Fourier transform of (1) reads:

$$\begin{aligned}
H = & \sum_{\vec{k}} a_{\vec{k}}^\dagger a_{\vec{k}} [E_a + 2t_2 (\cos \vec{k} \vec{a}_1 - \cos \vec{k} \vec{a}_2)] \\
& + \sum_{\vec{k}} b_{\vec{k}}^\dagger b_{\vec{k}} [E_b - 2t_2 (\cos \vec{k} \vec{a}_1 - \cos \vec{k} \vec{a}_2)] \\
& - t_1 \sum_{\vec{k}} a_{\vec{k}}^\dagger b_{\vec{k}} [e^{-i\gamma} (1 + e^{-i\vec{k}(\vec{a}_1 + \vec{a}_2)}) \\
& + e^{i\gamma} (e^{-i\vec{k}\vec{a}_2} + e^{-i\vec{k}\vec{a}_1}) + H.c.] . \quad (2)
\end{aligned}$$

By taking  $\{\vec{a}_1, \vec{a}_2\}$  along the Ox- and Oy-axis, respectively, and the zero energy such that  $E_a + E_b = 0$ , with the notations:

$$\begin{aligned}
f(\vec{k}) &= \cos k_x - \cos k_y, \\
g(\vec{k}) &= e^{-i\gamma} (1 + e^{-i(k_x + k_y)}) + e^{i\gamma} (e^{-ik_x} + e^{-ik_y}) \\
\Delta &= (E_a - E_b)/2, \quad (3)
\end{aligned}$$

the Hamiltonian (2) can be written in the matrix form:

$$H = \sum_{\vec{k}} \begin{pmatrix} a_{\vec{k}}^\dagger & b_{\vec{k}}^\dagger \end{pmatrix} \begin{pmatrix} \Delta + 2t_2 f(\vec{k}) & -t_1 g(\vec{k}) \\ -t_1 g^*(\vec{k}) & -\Delta - 2t_2 f(\vec{k}) \end{pmatrix} \begin{pmatrix} a_{\vec{k}} \\ b_{\vec{k}} \end{pmatrix} \quad (4)$$

The spectral properties and the symmetries of (4) can be conveniently analyzed by expressing the Hamiltonian  $H(\vec{k})$  in terms of Pauli matrices:

$$H(\vec{k}) = -t_1 \text{Reg}(\vec{k}, \gamma) \sigma_x + t_1 \text{Img}(\vec{k}, \gamma) \sigma_y + (\Delta + 2t_2 f(\vec{k})) \sigma_z, \quad (5)$$

where the coefficients show the properties:

$$\begin{aligned}
\text{Reg}(\vec{k}, \gamma) &= \text{Reg}(-\vec{k}, -\gamma), \\
\text{Img}(\vec{k}, \gamma) &= -\text{Img}(-\vec{k}, -\gamma), \\
f(\vec{k}) &= f(-\vec{k}). \quad (6)
\end{aligned}$$

It is of interest to notice that the spectrum of any Hamiltonian of the form (5) is symmetric around the energy  $\omega = 0$ , exhibiting this *electron-hole symmetry* no matter the parameters  $t_1, t_2, \gamma, \Delta$ . In order to prove the symmetry, it is sufficient to find an operator  $\mathcal{P}$  that anticommutes with the Hamiltonian. The existence of such an operator ensures that, if the eigenenergy  $\omega_{\vec{k}}$  belongs to the spectrum, the same is true for  $-\omega_{\vec{k}}$ , i.e., the energy spectrum is symmetric. Indeed, one checks easily that the operator

$$\mathcal{P} = \text{Img}(\vec{k}) \sigma_x + \text{Reg}(\vec{k}) \sigma_y \quad (7)$$

anticommutes with (5). More than this, the analytical expression of the eigenenergies can be obtained straightforward from (4):

$$\omega_{\pm}(\vec{k}) = \pm \sqrt{(\Delta + 2t_2 f(\vec{k}))^2 + t_1^2 |g(\vec{k}, \gamma)|^2}, \quad (8)$$

showing explicitly a symmetric two-branch spectrum.

A second peculiarity of the spectrum (8) is the *anisotropy*, which is manifest provided that  $\Delta \neq 0$ , and is due to the obvious relation  $f(k_x, k_y) = -f(k_y, k_x)$ .

The *time-reversal* (TR) symmetry of the model is controlled by the phase  $\gamma$ , associated to the nearest-neighbor hopping  $t_1$ . Indeed, the TR invariance condition  $H(\vec{k}) = H^*(-\vec{k})$  requires  $g(\vec{k}, \gamma) = g^*(-\vec{k}, \gamma)$ , while the function  $g$  defined in (3) exhibits  $g(\vec{k}, \gamma) = g^*(-\vec{k}, -\gamma)$ , proving that the time-reversal invariance of the Hamiltonian is guaranteed only for  $\gamma = 0$ .

In what concerns the *inversion* symmetry  $H(\vec{k}) = H(-\vec{k})$ , it is easy to see from (8) that the symmetry is fulfilled only if  $g(\vec{k}, \gamma) = 0$ .

The energy spectrum (8) describes either a *semimetal* or an *insulator*, depending on the considered point in the parameter space  $\{\gamma, \Delta, t_2\}$ , when  $t_1$  is taken for energy unit ( $t_1 = 1$ ).

Let us discuss first the occurrence of the semimetallic phase. The touching of the bands at  $\omega = 0$  occurs provided that the two terms under the square root in (8) vanish *simultaneously*. It is to distinguish three cases:

a) If  $\gamma = 0$ , the function  $g(\vec{k}, \gamma = 0)$  vanishes along two lines  $k_x = \pi$  and  $k_y = \pi$  in the BZ. Along the first line one has  $f(\pi, k_y) = -2\cos^2 k_y/2$ , resulting the dispersion

$$\omega_{\pm}(\pi, k_y) = \pm(\Delta - 4t_2 \cos^2 k_y/2). \quad (9)$$

Then, as long as  $0 < \Delta/4t_2 < 1$ , the condition  $\omega_{\pm}(\pi, k_y) = 0$  is satisfied at  $k_y = \pm 2\arccos \sqrt{\Delta/4t_2}$ , meaning that there are two points belonging to BZ where the bands touch each other, giving rise to the semimetallic phase. In the particular case  $\Delta/4t_2 = 1$ , the expression (9) vanishes at  $k_y = 0$ , meaning the existence of a single touching point in the BZ at  $\{k_x = \pi, k_y = 0\}$ . The same is obtained for  $\Delta = 0$ , the touching point being now  $\{k_x = \pi, k_y = \pi\}$ .

A similar discussion carried out for the other line ( $k_y = \pi$ ) indicates that, as long as  $\Delta$  and  $t_2$  are taken positive, the condition  $\omega = 0$  cannot be fulfilled along it.

b) If  $\gamma \neq 0$ , the function  $g(\vec{k}, \gamma)$  vanishes only at four points located at the edges of BZ, namely  $\vec{k}_{1,2} = (0, \pm\pi)$ ,  $\vec{k}_{3,4} = (\pm\pi, 0)$ . If we assume now  $\Delta = t_2 = 0$ , the band touching occurs at the four mentioned points, around which the energy dispersion is linear (see Fig.2), meaning in fact *two* cones per BZ.

c) If  $\gamma \neq 0$  and  $\Delta/4t_2 = 1$ , the band touching occurs only at the two points  $\vec{k}_3 = (\pi, 0)$ ,  $\vec{k}_4 = (-\pi, 0)$ , where  $f(\vec{k}) = -2$ , resulting a semimetal with a *single* cone per BZ. (As observed also by Hou [10], the cone position in BZ depends on the sign of  $\Delta$ . So, if  $\Delta/4t_2 = -1$ , the band degeneracy occurs now at  $\vec{k}_1, \vec{k}_2$ , the spectrum being rotated with  $\pi/2$  compared to the other case.)

Except for the above mentioned cases the energy spectrum is gapped. However, it is to find out under what circumstances the insulating phase is a topological one. A specific feature of the model is that the time-reversal symmetry breaking is necessary, but not sufficient, for the appearance of the topological insulator phase. The reason is that the phase  $\gamma$  breaks indeed the TR symmetry, but cannot open the gap. The statement in the case c) above says that the existence of the gap requires  $\Delta \neq 4t_2$ , meaning that either  $\Delta$  or  $t_2$  must be different from zero.

Based on the calculation of the Chern number, a topological phase showing anomalous quantum Hall effect is predicted in [10] under the condition  $\Delta/4t_2 < 1$ , which implies that  $t_2$  should be the non-vanishing parameter. In the opposite case ( $\Delta/4t_2 > 1$ ), the system behaves as a conventional bulk insulator. In the next sections, this problem will be analyzed in terms of the spectral properties of confined systems, by looking for topologically protected edge states in the ribbon (strip) and plaquette geometry.

### EDGE STATES IN THE RIBBON GEOMETRY

We study two kinds of ribbons obtained by cutting the edges in different manners: parallel to the A-A and A-B direction, respectively, the angle between the two directions being  $\pi/4$ . The intention is to detect the differences, if any, in the spectral properties coming from the different atomic connectivities at the ribbon edges in the two cases. Since the ribbon cut along the A-A chain ends with a B-B chain, this type of ribbon will be called in what follows as the AA/BB ribbon. The other ribbon gets the both cuts along the same type of chain, and it will be called the AB/AB ribbon.

Technically, one has to choose the unit cell in two different ways corresponding to the two types of ribbons (see Fig.3). Next, one performs the Fourier transform of

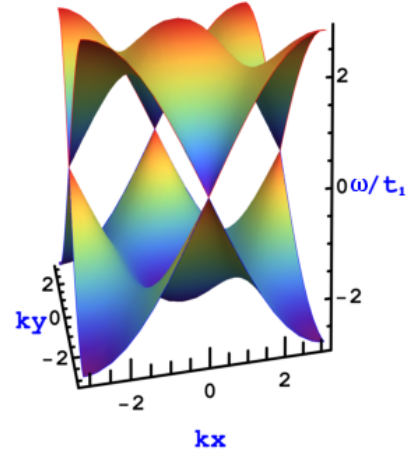


FIG. 2: (Color online) The semimetallic case b) in the text showing band touching for  $t_2 = \Delta = 0, \gamma = \pi/4$ .

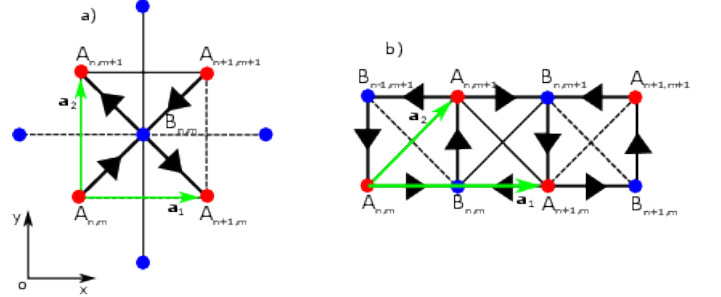


FIG. 3: (Color online) The unit cells defined by the vectors  $\vec{a}_1$  and  $\vec{a}_2$  (in green) for the ribbon cut parallel to A-A atomic chain in (a), and parallel to A-B chain in (b).

the Hamiltonian along the direction parallel to edges, and then, the ribbon energy spectrum is calculated by numerical diagonalization. Still, the existence of the flat edge states shown by the AA/BB ribbon in Fig.4a is proved analytically.

The presence of topologically protected or dissipative edge states in a gapped spectrum is a rather common feature of confined 2D systems. However, in this section, we prove the existence of *dispersive* current-carrying edge states in the *gapless* phase of the ribbon, which seems to be a new conceptual aspect in the frame of topological states.

The discussion of the spectral properties in the ribbon geometry will be carried out in several steps. First, we confirm the semimetal phase, and next we consider the insulating phases. The rather many possible cases are summarized at the end of the section in the phase diagram Fig.8.

It turns out that the semimetal exists under the same constraints as for the infinite system:

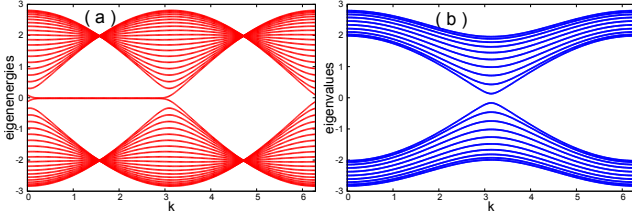


FIG. 4: (Color online) Semimetallic spectrum under the conditions  $t_2 = \Delta = 0$ ,  $\gamma = -\pi/4$  for the AA/BB (in red) and AB/AB (in blue) ribbons. The width is  $M = 20$  unit cells.

1. in the case  $\gamma \neq 0$  and  $\Delta = t_2 = 0$  (similar to the case b) in the discussion of the infinite lattice), the semimetallic character is revealed by the both types of ribbons, although there are non-trivial differences between them, obvious in Fig.4. For instance, the flat band at  $E = 0$  in the spectrum of the AA/BB-ribbon shows a striking similarity to the case of the well-known zig-zag graphene ribbon [15]. We show in what follows that the flat band is composed of edge states, which occur at any momentum  $k \in [0, \pi]$  no matter the value of the phase  $\gamma$ . To this end, we perform the Fourier transform of the Hamiltonian (1) along the  $ox$ -axis (parallel to AA-edge) and impose vanishing boundary conditions on the perpendicular direction. The resulting Hamiltonian for the AA/BB-ribbon reads:

$$H(k) = \sum_{m=1}^M (\Delta + 2t_2 \cos k) [a_{km}^\dagger a_{km} - b_{km}^\dagger b_{km}] - t_2 \sum_{m=1}^M [a_{km}^\dagger a_{km+1} - b_{km}^\dagger b_{km+1} + H.c.] - t_1 \sum_{m=1}^M [a_{km}^\dagger b_{km} (e^{-i\gamma} + e^{i\gamma - ik}) + a_{km}^\dagger b_{km-1} (e^{i\gamma} + e^{-i\gamma - ik}) + H.c.] , \quad (10)$$

where the index  $m$  counts the unit cells along the ribbon width. (The AB/AB-ribbon can be addressed similarly.)

Looking for the eigenfunctions of (10) as

$$|\Psi(k)\rangle = \sum_m (\alpha_{km} a_{km}^\dagger + \beta_{km} b_{km}^\dagger) |0\rangle, \quad (11)$$

in the case under discussion ( $\Delta = t_2 = 0$ ), the coefficients satisfy the following linear equations ( $t_1 = 1$ ):

$$\begin{aligned} -(e^{i\gamma} + e^{-i\gamma + ik})\alpha_{km} + (e^{-i\gamma} + e^{i\gamma + ik})\alpha_{km+1} &= E(k)\beta_{km} \\ -(e^{-i\gamma} + e^{i\gamma - ik})\beta_{km} + (e^{i\gamma} + e^{-i\gamma - ik})\beta_{km-1} &= E(k)\alpha_{km}. \end{aligned} \quad (12)$$

We are interested in the behavior of the wave function at  $E = 0$ , where Eq.(12) gives

$$\alpha_{k,m} = x^{m-1} \alpha_{k,1}, \quad x = \frac{e^{i\gamma} + e^{-i\gamma + ik}}{e^{-i\gamma} + e^{i\gamma + ik}}. \quad (13)$$

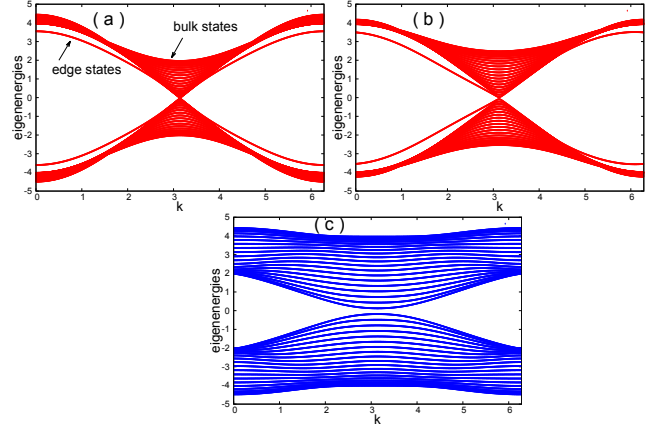


FIG. 5: (Color online) Semimetallic spectrum under the conditions  $t_2 = 0.5$ ,  $\Delta = 2$ . Branches consisting of edge states are visible for the AA/BB ribbon (in red). The branches are symmetric in (a) at  $\gamma = 0$ , and become asymmetric in (b) at non-vanishing phase ( $\gamma = \pi/8$ ). The AB/AB ribbon does not exhibit such features (the case  $\gamma = 0$  is shown in (c)).

Under the condition  $|x| < 1$ , the coefficient  $\alpha_{km}$  shows the maximum value at the edge  $m=1$  and decays monotonically versus the other edge  $m=M$ . (It is trivial to show that  $\beta_{km}$  behaves oppositely.) One concludes that the wave function  $|\Psi(k)\rangle = \sum_m \alpha_{km} a_{km}^\dagger |0\rangle$ , corresponding to the eigenvalue  $E(k) = 0$ , describes an edge state localized near the edge  $m = 1$ . Since  $|x|^2 = (1 + \cos(2\gamma - k))/(1 + \cos(2\gamma + k))$ , the condition  $|x| < 1$  can be easily rewritten as  $\sin(2\gamma)\sin k < 0$  and is satisfied for any  $k$  in the range  $[0, \pi]$ , if  $\gamma$  is assumed to be negative. This result confirms the numerical data shown in Fig.4a.

One has to comment for the sake of accuracy that, as it is known for such kind of problems [15], the perfect degeneracy at  $E = 0$  occurs only in the limit of infinite wide ribbon ( $M \rightarrow \infty$ ), otherwise the spectrum remains quasi-degenerate. The reason for such a behavior is the superposition of the edge states localized near opposite edges, which although small is still non-zero at finite width [16].

2. The semimetallic character is preserved along the line  $\Delta/4t_2 = 1$  no matter whether the TR symmetry is broken ( $\gamma \neq 0$ ) or not ( $\gamma = 0$ ). The situation is similar to the cases a) and c) discussed previously for the infinite lattice. Again, this is true for both ribbons, existing however qualitative differences illustrated in Fig.5.

The important finding in this case is that the AA/BB-ribbon exhibits dispersive edge modes as shown in Fig.5a and Fig.5b. Since the spectrum is gapless, inevitably, these modes are energetically embedded in the continuum of the bulk states. So, we notice in the panels (a) and (b) of Fig.5 that some eigenvalues are organized in branches which are detached from the rest of the spectrum. This feature is missing for the AB/AB ribbon (Fig.5c).

The geometrical localization of the corresponding wave



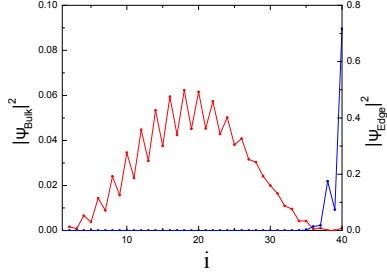


FIG. 6: (Color online) The local distribution of two wave functions at  $E \simeq -1$  in the semimetallic phase for the AA/BB ribbon with  $M=20$  cells: the edge state (blue) at  $k = 0.72 \times \pi$  and the bulk state (red) at  $k = 0.82 \times \pi$ . The index 'i' counts the sites along the ribbon width (other parameters:  $t_2 = 0.5, \Delta = 2, \gamma = \pi/8$ ).

functions can be inspected by calculating  $|\langle i|\Psi\rangle|^2$ , meaning the projection of the wave function  $|\Psi\rangle$  on the lattice sites  $i$  along the width of the ribbon. Fig.6 shows that such a state (shown in blue) is peaked at the ribbon edge, while a state in the bulk (shown in red) covers the middle of the ribbon.

Another significant observation is the symmetry of the edge state branches around  $k = \pi$  at  $\gamma = 0$  in Fig.5a. The meaning is that, at any energy  $E$ , there are two states of opposite velocity  $dE/dk$  at the same edge, resulting a vanishing total current carried along edges. On the other hand, if  $\gamma \neq 0$  as in Fig.5b, the edge state branches become asymmetric, and non-vanishing currents, running in opposite directions along the two edges, are allowed. In other words, the AA/BB-ribbon with n.n.n. hopping and broken TR symmetry, supports chiral edge states even in the semimetallic phase. The fate of these states in the case of finite size plaquettes will be examined in Sec.IV.

3. Finally, we look for the Chern insulating phase in the ribbon geometry, distinguished by the presence of chiral edge states in a *gapped* spectrum. The spectra in Fig.7 demonstrate that the breaking of the TR symmetry (i.e.,  $\gamma \neq 0$ ) is not sufficient for the occurrence of the Chern insulator. Indeed, there is a separation line  $\Delta/4t_2 = 1$  above which the system is a conventional bulk insulator (as in the panels (c) and (d)), while below it (for  $\Delta/4t_2 < 1$ ) the system becomes a topological insulator. The result indicates that the existence of the edge states in the gap is dictated by two conditions:  $\gamma \neq 0$  and  $t_2 \neq 0$ . This behavior is the same for the both types of ribbon, and one has to note that the separation line is that one along which the system becomes a semimetal.

However, one has still to decide whether the states are protected or not against the backscattering. To this end, we observe that the edge states indicated by "1" and "2" in Fig.7a are running at the same energy in opposite directions (i.e., show different chirality), but prove to be located at *opposite* sides of the ribbon. Then, one con-

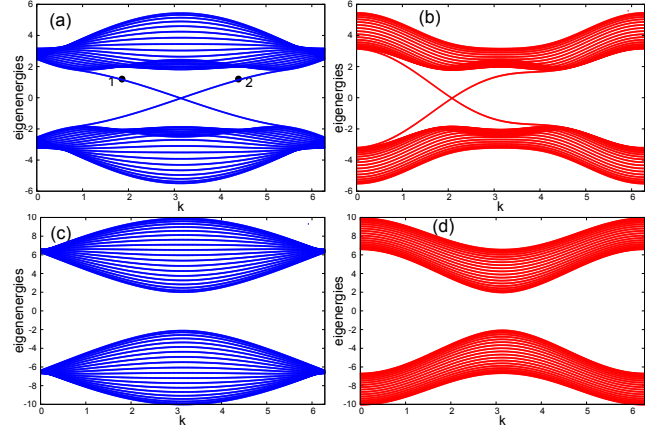


FIG. 7: (Color online) (a), (b): The ribbon energy spectrum as function of the momentum  $k$  in the Chern insulating phase showing edge states in the gap ( $\gamma = \pi/4, t_2 = 1, \Delta = 1.5$ ). (c), (d): The spectrum in the conventional insulating phase ( $\gamma = \pi/4, t_2 = 1, \Delta = 6$ ). The spectra for AB/AB ribbon are presented in blue, those for AA/BB ribbon are in red)

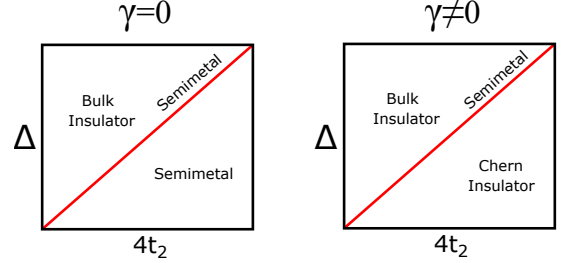


FIG. 8: The phase diagram in the space of relevant parameters  $\{\Delta, t_2\}$ , with and without time-reversal symmetry (left and right panel, respectively).

cludes that they are robust against elastic processes and cannot undergo backscattering.

The results concerning the spectral properties are collected in the phase diagram Fig.8.

## PLAQUETTE GEOMETRY: EDGE STATES AND ANOMALOUS QUANTUM HALL EFFECT

The attention will be focused now on the transport properties and disorder effects, the study being carried out in finite size (plaquette) geometry. One starts with the spectral properties of the plaquette, and continues with the calculation of the Hall effect for clean and disordered systems.

1. *Spectral properties.* In the previous section, we identified edge states in the ribbon geometry, when vanishing boundary conditions are applied along one direction only. Our goal now is to examine the edge states in the more physical situation of confined systems obtained by imposing vanishing conditions all around the perimeter. Actually, such a plaquette is obtained by cutting the ribbon

perpendicularly, but taking care to ensure a vanishing flux through the plaquette area. One gets two types of plaquettes: with AB and AA (or BB) atomic sequence along the perimeter, respectively.

We expect to get edge states running along the boundary at least in some range of parameters. One may also anticipate that, in case of broken TR symmetry, the edge states would get chirality and support *anomalous* quantum Hall effect, detectable in a four-lead Hall device. This picture corresponding to a description in terms of edge states of the Chern-type topological insulator is developed in what follows.

In what concerns the spectral properties of the finite system, we start underlying the relevance of the case  $\Delta/4t_2 = 1$ , which appeared to be important in the previously discussed geometries. Fig.9a, which shows the dependence of the spectrum on  $\Delta/4t_2$  at  $\gamma \neq 0$ , is illustrative in this respect: one notices that the gap is filled with (edge) states if  $\Delta/4t_2 < 1$  and it is clean in the opposite case. This demonstrates the transition from the Chern topological insulator to the conventional insulator, crossing the situation where the gap closing indicates a semimetal. The chirality and robustness of the edge states will be discussed below.

The dependence of the energy spectrum on the phase  $\gamma$  is depicted in Fig.9b, in the regime  $\Delta/4t_2 < 1$ . This description is the analog of the Hofstadter-type energy spectrum of the *confined* 2D electron gas, expressed as function of the external magnetic flux. Because of this analogy, we shall equivalently call the phase  $\gamma$  as a 'local-flux'. However, instead of the butterfly picture created by the sequence of bands and gaps in the Hofstadter spectrum, the spectrum in Fig.9b contains a single gap and exhibits a 'binocular' aspect.

The eigenvalues as function of  $\gamma$  are obtained by the numerical diagonalization of the Hamiltonian matrix. Besides the electron-hole symmetry, some other properties are notable in Fig.9b: i) the spectrum is periodic with the period  $\delta\gamma = \pi$ , ii) the spectrum shows mirror symmetry around  $\gamma = \pi/2$ , iii) the gap vanishes at  $\gamma = 0, \pi/2$  where the system becomes semimetallic, iv) the gap width depends on the 'local-flux' and reaches its maximum at  $\gamma = \pi/4$  and  $3\pi/4$ .

The emergence of chiral edge states in the gap is the major property of the energy spectrum of the finite plaquette in the case  $0 < \Delta/4t_2 < 1$ . The edge character can be shown as in the ribbon case by calculating numerically the electron distribution  $|\langle i|\Psi\rangle|^2$  for any state  $|\Psi\rangle$  in the gap, where  $i$  stands for any lattice site of the plaquette. It turns out that, indeed, the gap states are located near the boundaries, such a state being depicted in Fig.10.

The confirmation of the chirality, meaning that the edge states carry the electron current in a given (clock/anticlockwise) direction, can be achieved by showing the *one-way* behavior of the transmission coefficients

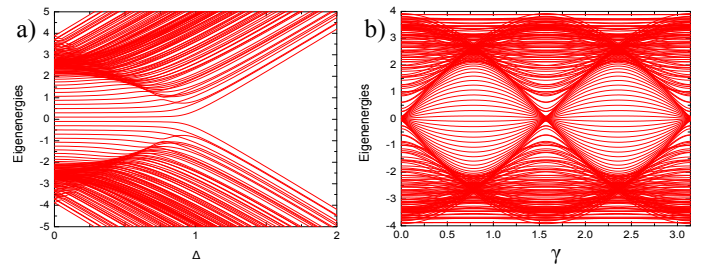


FIG. 9: (a) The energy spectrum of AB plaquette as function of the staggered energy  $\Delta$  (in units  $4t_2$ ) at  $\gamma = \pi/4$ . (b) The energy spectrum as function of the phase  $\gamma$  at  $\Delta = 0, t_2 = 1$ .

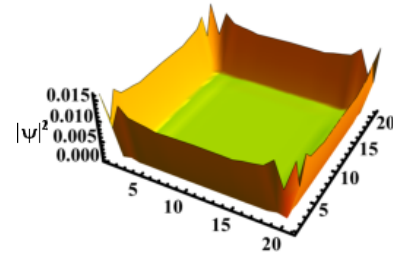


FIG. 10: (Color online) Electron density  $|\Psi(r)|^2$  corresponding to the edge state at  $E = -1.21379$  for an AB plaquette of dimensions  $21 \times 20$  cells ( $\gamma = \pi/4, \Delta = 0$ ).

in the four-lead Hall device, which is the suitable arrangement for investigating the transport properties.

2. *Transport properties.* The goal is now to calculate the transverse (Hall) conductance presumed to be non-zero by reason of time-reversal breaking induced by the local flux  $\gamma$ . On the other hand, one has to keep in mind that the total flux through the plaquette vanishes. Then, an eventual integer value of the Hall conductance obtained by the calculation would confirm the anomalous quantum Hall effect carried by chiral edge states located in the gap of a Chern insulator.

In order to do that, we simulate a Hall device by attaching four leads to the plaquette and apply afterwards the Landauer-Büttiker formalism. The role of the leads is to inject current in the system and to enable the measuring of voltages. The approach requires the knowledge of the full Hamiltonian that describes the finite plaquette, the leads and the coupling between them. The electron transmission coefficients  $T_{\alpha,\beta}$  between different leads (indexed by  $\alpha, \beta$ ) can be expressed in terms of the retarded Green function, which has to be calculated explicitly. Once  $T_{\alpha,\beta}$  are known, the transverse (Hall)  $R_H$  resistance is given immediately by the formalism. The technical details of the calculation can be found in extenso in [19], for instance, and will not be repeated here.

The Hall transport is studied in the Chern insulating phase and the semimetallic phase, which have been noticed in Fig.9a. The non-vanishing Hall conductance results from the asymmetry of the transmission coefficients

$T_{\alpha,\alpha+1} \neq T_{\alpha+1,\alpha}$ , induced in its turn by the phase  $\gamma$  that breaks the TR symmetry.

In the energy range occupied by the edge states, the numerical calculation indicates that the asymmetry is total, i.e.,  $T_{\alpha,\alpha+1} = 1, T_{\alpha+1,\alpha} = 0$ , meaning that the current is carried in a given direction (imposed by the sign of  $\gamma$ ). This fact expresses the chirality of the edge states and the lack of backscattering in the transport process for the model under consideration. Combined with the observation that all the other transmission coefficients  $T_{\alpha,\beta}$  vanish, in line with the Landauer-Büttiker theory, the consequence is a *quantized* Hall conductance. In Haldane's terminology, this quantization is *anomalous*, as it occurs in the absence of the external magnetic field.

The numerical results supporting the above statements are shown in Fig.11, obtained under the condition  $\Delta/4t_2 < 1$ , which, as already shown in Fig.9, induces edge states in the insulating phase. The calculation is performed for a plaquette with all the four edges of the AB-type. The arrangement of the leads in the Hall device is sketched in Fig.11(right). A gate potential can be applied on the plaquette allowing the scanning all energies  $E$  in the spectrum.

As evident in Fig.11, as long as  $\gamma$  crosses the gap, the transmission coefficient  $T_{21}$  vanishes in the left gap, but manifests perfect transmission ( $T_{21} = 1$ ) in the right one. Since the transmission  $T_{12}$  behaves vice-versa, one concludes that the edge states exhibit opposite chirality in the two sectors of the 'binocular' spectrum. Accordingly, the Hall resistance is  $R_H = \pm h/e^2$ , the sign being different in the two sectors. In Fig.11, the blue curve corresponds to  $E = 0$ , the red curve to  $E = 1$ , the difference in appearance coming from the different ranges occupied (on the  $\gamma$ -axis) by the edge states at the two energies (one may check with Fig.9b).

The next task is to prove the robustness of edge states against disorder, which is the fingerprint of their topological character. The topic is addressed in what follows in conjunction with the transport properties of the semimetal. In the semimetallic phase, reached under the conditions  $\Delta/4t_2 = 1$  and  $\gamma \neq 0$ , the calculation of the Hall resistance reveals a new conceptual aspect. It refers to the disorder-driven AQHE arising in the semimetallic phase.

Similar to the situation met in Fig.8 for the ribbon geometry, the energy spectrum of the confined system in the semimetallic phase exhibits edge states intercalated among the bulk states. However, any perturbation, including the plaquette-lead coupling, affects the spectral properties, giving rise to the hybridization of the two types of states. This yields backscattering and impedes the quantization of the transport response. With the purpose of reducing the hybridization, we introduce disorder, which induces localization and hence reduces the superposition of the two kinds of states.

According to the Anderson's localization theory [17,

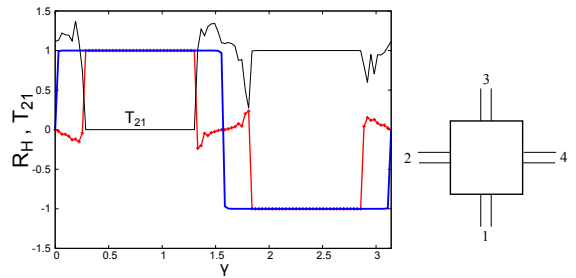


FIG. 11: (Color online) Hall resistance versus the 'local flux'  $\gamma$  in the Chern insulating phase ( $t_2 = 1, \Delta = 0$ ) for two values of the Fermi level  $E_F = 0$  (blue) and  $E_F = 1$  (red). As an example, transmission  $T_{21}$  is also shown for  $E_F = 1$ . The quantization is manifest in the range occupied by the edge states (check with Fig.9b). (Calculation is performed for a  $25 \times 25$  unit cells plaquette of AB type, with four leads attached in crossed geometry as sketched on the right.)

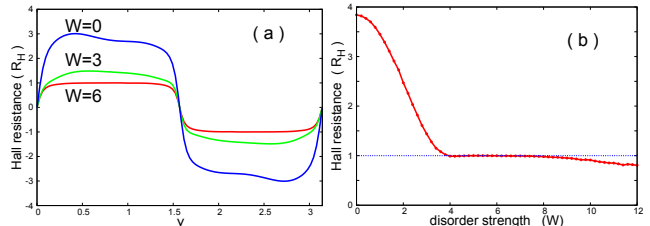


FIG. 12: (Color online) Disorder effect on the Hall resistance in the semimetallic phase ( $t_2 = 1, \Delta = 4; E = 0$ ). (a)  $R_H$  as function of  $\gamma$  for different disorder strengths  $W$ . (b)  $R_H$  as function of  $W$  at  $\gamma = \pi/4$ . The trend towards resistance quantization with increasing disorder is observed in both panels (plaquette dimension is  $15 \times 15$  unit cells, average is performed over 1000 disorder configurations; data are obtained for disordered AB-plaquette in panel (a), and AA-plaquette in (b)).

18], all quantum states in the *infinite* two-dimensional systems are localized, irrespective how weak the disorder is. On the other hand, in the finite-sample, the 1D states (the edge states in our case) should localize first, and the 2D bulk states afterwards (The difference comes from the different localization length  $\lambda$  of the two types of states, which has to be compared to the typical dimension  $L$  of the sample). This should be true only if the 1D states under discussion are not protected against disorder. However, in our case, the attention signal comes from the calculation of the Hall resistance that reveals the tendency toward quantization  $R_H = \pm 1h/e^2$  as the disorder in the system is increased gradually.

In Fig.12a we show the Hall resistance for different strengths of the Anderson disorder characterized by the range  $[-W, W]$ , in which the diagonal energies of the tight-binding Hamiltonian are randomly distributed. It is to observe the evolution of the curve  $R_H(\gamma)$  from the ordered case  $W = 0$  to the disordered one  $W = 6$ , which shows the quantum plateau (red curve). The dependence



on disorder can be remarked also in Fig.12b, where  $R_H$  is calculated as function of the disorder strength  $W$  at fixed  $\gamma = \pi/4$ . The topological behavior  $R_H = 1$  is reached at  $W \approx 4$  (for the given plaquette dimensions), while at very strong disorder the Hall plateau is spoiled, as it should.

This outcome demonstrates that, in the disordered semimetal, the states in the bulk become localized and do not contribute to the transport process, while the edge states are robust against disorder and give rise to the anomalous quantum Hall effect.

## CONCLUSIONS

In conclusion, in the frame of a confined diatomic lattice model with broken time-reversal symmetry and hopping to the next-nearest-neighbors, we have proved the occurrence of chiral edge states, robust to disorder, which may exist in the absence of an external magnetic field. The states are the physical support for the anomalous quantum Hall effect.

The case of the infinite lattice allows the exact diagonalization of the Hamiltonian in the momentum space, such that different phases (semimetallic, conventional insulator or Chern insulator) can be identified from the expression of the energy spectrum and the Hamiltonian symmetries. The spectral properties depend on the set of parameters  $\gamma$  (which controls the time-reversal),  $t_2$  (n.n.n.hopping), and  $\Delta$  (atomic energies staggering). The electron-hole, time-reversal, and inversion symmetries are discussed. The diatomic lattice with n.n.n. hopping is an example of non-bipartite lattice that exhibits a symmetric spectrum around the zero energy. The energy spectrum of the semimetallic phase may exhibit one or two touching points, depending on the circumstances discussed in Sec.II.

The question under discussion is how the boundary conditions affect the spectral properties, and more precisely, whether the confinement may give rise to chiral edge states that should be the support of the quantum anomalous Hall effect.

In first instance, the boundary effect is noticed in the ribbon (strip) geometry. We tailor the ribbons in two different ways, obvious in Fig.1, which are called AA/BB and AB/AB ribbons, respectively. The notable results are : i) the presence of the degenerated flat band composed by edge states in the AA/BB ribbon (Fig.4a), ii) the occurrence in the semimetallic phase of edge states embedded in the continuum of the bulk states (Fig.5a and b), iii) the emergence of chiral edge states in the insulating phase of both ribbons if  $\Delta/4t_2 < 1$  (Fig.7a and b). All these situations are presented in the phase diagram Fig.8.

The finite size plaquette geometry allows for the calculation of the transport properties and disorder effects.

The plaquette has a rectangular shape, and can be obtained by cutting the ribbon perpendicularly. One has to pay attention to the requirement of zero total flux through the plaquette. By attaching four semi-infinite leads one simulates a Hall device, and the Hall resistance is calculated numerically following the Landauer-Büttiker recipe.

The energy spectrum of the isolated plaquette as function of the phase  $\gamma$  shows a 'binocular' structure, whose gap is filled with edge states if  $\Delta/4t_2 < 1$  (Fig.9), and is empty in the opposite case. By calculating the Hall resistance, it turns out that the edge states generated by the model are chiral and responsible for the anomalous quantum Hall effect (Fig.11).

The semimetallic phase, occurring under conditions  $\gamma \neq 0$  and  $\Delta/4t_2 = 1$ , deserves special attention. Being characterized by intercalated edge and bulk states, it cannot exhibit quantized transport as long as the bulk states are carrying electrons. By using Anderson disorder, we succeed to localize the bulk states and, at the same time, to observe a quantized Hall resistance at sufficiently strong disorder (Fig.12). This says that the edge states we have evidenced in the semimetallic phase are chiral and robust against disorder. We call this effect as *disorder-driven* anomalous quantum Hall effect.

## ACKNOWLEDGMENTS

We acknowledge financial support from the Core Program PN18-11 and grant PNIII-P4-ID-PCE-2016-0084 of the Romanian Ministry of Research and Innovation. We are much indebted to M. Tolea for useful discussions.

- 
- [1] F.D.M. Haldane, Phys. Rev. Lett. **61**, 2015 (1988).
  - [2] E. V. Castro, M. P. Lopez-Sancho, and M. A. H. Vozmediano, Phys. Rev. B **92**, 085410 (2015).
  - [3] E. Prodan, T. L. Hughes, and B. A. Bernevig, Phys. Rev. Lett. **105**, 115501 (2010).
  - [4] T. Neupert, L. Santos, C. Chamon, and C. Mudry, Phys. Rev. Lett. **106**, 236804 (2011).
  - [5] D. N. Sheng, Zheng-Cheng Gu, Kai Sun, and L. Sheng, Nat. Commun. **2**,389 (2011).
  - [6] N. Hao, P. Zhang, Z. Wang, W. Zhang, and Y. Wang, Phys. Rev. B **78**, 075438 (2008).
  - [7] E.Fradkin, *Field Theories of Condensed Matter Physics*, second edition, p.714, Cambridge University Press, 2013.
  - [8] C. L. Kane and E. J. Mele, Phys. Rev. Lett. **95**, 226801 (2005).
  - [9] Y.Hatsugai, J.Phys.: Condens. Matter **9**, 2507 (1977).
  - [10] J.M. Hou, Phys. Rev. Lett. **111**, 130403 (2013).
  - [11] P. Sessi, D. Di Sante, A. Szczerbakow, F. Glott, S. Wilfert, H. Schmidt, T. Bath P. Dziawa, M. Greiter, T. Neupert, G. Sangiovanni, T. Story, R. Thomale, M. Bode, Science, **354**, 1269 (2016).
  - [12] A. Mielke, Phys. Lett. A **174**, 443 (1993).

- [13] We shall see in Fig.9b that inside the gap  $dE/d\gamma$  changes its sign, but Fig.11 says that the Hall effect keeps a given sign. This says that the derivative of the energy with respect to the phase  $\gamma$  cannot be identified with the chirality of the edge state.
- [14] M. Büttiker, Y. Imry, R. Landauer, and S. Pinhas, Phys. Rev. B **31**, 6207 (1985).
- [15] K. Wakabayashi, M. Fujita, H. Ajiki, and M. Sigrist, Phys. Rev. B **59**, 8271 (1999).
- [16] B. Ostahie and A. Aldea, Phys. Rev. B **93**, 075408 (2016).
- [17] E. Abrahams, P. W. Anderson, D. C. Licciardello, and T. V. Ramakrishnan, Phys. Rev. Lett. **42**, 673 (1979).
- [18] D. Vollhardt, and P. Wölfle, Phys. Rev. Lett. **45**, 842 (1980).
- [19] B. Ostahie, M. Nita, and A. Aldea, Phys. Rev. B **91**, 155409 (2015).